Enhanced electrocatalysts fabricated via quenched ultrafast sintering: physicochemical properties and water oxidation applications

Antonino Curcio[a], Matthew J. Robson[a], Alessio Belotti[a], Zhiwei Hu[b], Yi-Ying Chin[c], Chien-Te Chen[d], Hong-Ji Lin[d], and Francesco Ciucci[a,e,*]

[a] Department of Mechanical and Aerospace Engineering, The Hong Kong University of Science and Technology, Hong Kong, China

[b] Max Planck Institute for Chemical Physics of Solids, Nothnitzer Strasse 40, Dresden 01187, Germany

[c] Department of Physics, National Chung Cheng University, Chiayi 62102, Taiwan

[d] National Synchrotron Radiation Research Center, 101 Hsin-Ann Road, Hsinchu 30076, Taiwan

[e] Department of Chemical and Biological Engineering, The Hong Kong University of Science and Technology, Hong Kong, China

[*] Corresponding author: francesco.ciucci@ust.hk

Phone: +852 2358 7187

Fax: +852 2358 1543

Abstract

The synthesis of transition metal oxides is typically time- and energy-consuming. Recently, fast sintering methods have demonstrated great potential to reduce ceramic sintering time and energy use, improving the commercial prospects of these materials. In this article, a quenched ultrafast high-temperature sintering (qUHS) technique is developed to sinter metastable brownmillerite $SrCoO_{2.5}$ (SCO) in less than a minute. Surprisingly, SCO fabricated by qUHS shows higher activity for the oxygen evolution reaction (OER) compared to solid-state-reaction-synthesized SCO. Comparing samples produced by these two techniques, the increased OER performance of SCO qUHS is likely due to the synergistic combination of surface Co chemical state, higher mesoporosity and enhanced hydroxyl ion (OH^-) adsorption. This work demonstrates the potential of qUHS for producing high-performance electrocatalysts and provides detailed insights into the impact of ultrafast sintering on the materials' physical properties and electrocatalytic activity.

1 Introduction

Transition metal oxides such as perovskites are extensively used for many applications in the energy storage and conversion field, including electrocatalysis. However, the production of these materials is typically time- and energy-intensive,[1] increasing costs and limiting material throughput. Recently, rapid sintering techniques with reduced energy consumption [2] such as flash sintering,[3] microwave sintering,[4] spark plasma sintering,[5] cold sintering,[6] and ultrafast high-temperature sintering (UHS)[7] have attracted attention. These methods are characterized by fast heating rates, which lead to substantially shortened sintering times (from days or hours to minutes or seconds) and significant energy savings. However, the applicability of these rapid synthesis techniques is influenced by the ceramic's properties (*e.g.* electrical or absorption properties), and complex apparatuses with precise atmospheric and pressure control are required.[5-6] In contrast, UHS is independent of the material's properties[7] and its setup is simple, requiring only a power source and carbon fiber strips. In addition, the rapid heating rate (~10^4–10^5 °C/min) of UHS can suppress grain growth and reduces the volatilization of light chemical elements.[7-8]

As UHS is a novel technique, there is significant scope for development. For instance, UHS achieves a fast and tunable heating rate. However, it relies on ambient cooling. UHS can thus be augmented by a quenching step, which could expand the applicability of this technique to phases metastable at room temperature, such as some brownmillerite oxides.[9] In addition, UHS and similar fast sintering techniques are understood as far-from-equilibrium processes,[7] potentially resulting in materials with nonequilibrium defect distributions and non-standard physical properties.[7, 10] Consequently, further studies on the UHS process, the properties of materials synthesized by UHS, and their applications are needed. Areas of particular interest addressed by this article include the augmentation of UHS with a quenching step and the comparison of properties between UHS and conventionally sintered materials. Furthermore, at

the time of writing, UHS has mostly been used to produce battery electrolytes.[7, 11] Therefore, using UHS to fabricate electrocatalysts for the oxygen evolution reaction (OER), which is the performance-limiting reaction step in many electrochemical devices,[12] is novel and of substantial interest.

In this work, a quenched ultrafast high-temperature sintering (qUHS) technique was designed to enable the synthesis of metastable materials. To demonstrate this technique, brownmillerite $SrCoO_{2.5}$ (SCO) was chosen as a model material, as quenching is a key step in its synthesis. In addition, SCO has been widely studied as an electrocatalyst for the oxygen evolution reaction (OER),[13] allowing the influence of qUHS on OER performance to be studied. SCO is most often sintered using a conventional solid-state reaction technique[9, 14] and only in a few cases by a citrate or co-precipitation method.[14d, 15] For this reason, synthesis of SCO by solid-state reaction was chosen as a reference technique, hereafter referred to as the "conventional" route. To the best of the authors' knowledge, the above-mentioned rapid-sintering techniques have not been used to produce SCO.

SCO was synthesized by qUHS within a far shorter time (~15-30 seconds) than a conventional process (longer than 48 hours), which consists of several calcination and annealing steps before quenching.[9] Surprisingly, the OER performance of SCO produced by qUHS was also found to be substantially higher. This enhanced performance was attributed to the combination of a greater mesoporous network (~100-fold higher total pore volume), increased pore diameter (33.2 *vs* 17.74 nm) and enhanced OH^- adsorption in SCO qUHS, which synergistically improved hydroxyl ion transport. The effect of post-synthesis treatments (acid etching, and post-synthesis milling), and modified pre-sintering conditions (precursor grinding and pellet pressing) on the OER performance of SCO were also assessed.

In this report, for the first time, the suitability of qUHS for synthesizing metastable materials is demonstrated. In addition, the origin of the produced material's improved performance is investigated, contributing to the understanding of the influence of this sintering technique. This work represents a crucial step in the field of electrocatalysis by promoting qUHS and UHS for the rapid exploration of alternative materials compositions and metastable phases.

2 Methods

2.1 Materials' synthesis

Brownmillerite SCO was synthesized by solid-state reaction and qUHS. For both synthetic routes, $SrCO_3$ (Xilong Scientific, China) and Co_3O_4 (Shanghai Zhanyun Chemical, China) precursors were used. Precursor powders were mixed and ground with absolute ethanol (Sigma-Aldrich) using either a Tencan (XQM-0.4A, Tencan) or a Retsch (PM-100, Retsch) ball-miller. After ball-milling, precursor slurries were dried for 1 hour at 140°C and the collected powders were pressed into green pellets. For solid-state reaction synthesis, the pellets were first calcined for 24 hours at 1000°C and then for 24 hours at 900°C.[9] Finally, the disks were quenched, as reported in our prior work.[14i] In contrast, the qUHS method only involves the insertion of the green pellet between two carbon fiber strips (~100 mm in length, ~25 mm in width, and 2.5 mm in thickness), whereupon it is sintered for 15 to 30 s at a power of ~360 W, and subsequently dropped into a cooling tank for quenching. The sintered pellets obtained by solid-state reaction and qUHS were then thoroughly ground in an agate mortar.

2.2 Physical characterizations

The particle size distribution of the precursors and the SCO powders was measured by dynamic light scattering (DLS), using a Microtrac particle size analyzer (Microtrac Bluewave S3500). The crystal structure of the materials was analyzed using an X-ray diffractometer (PANalytical Model X'pert Pro) with Cu K-alpha radiation (λ=1.5406 Å). FT-IR measurements (Bruker Vertex 70 Hyperion 1000) after exposure to an alkaline solution (0.1 M KOH) were used to

assess the OH^- adsorption of SCO. The N_2 adsorption-desorption isotherms were measured using a Quantachrome Autosorb-1 instrument. Before testing, the powders were outgassed for 4 hours at 200 °C. The sample pore size distribution was evaluated using the Barrett-Joyner-Halenda (BJH) method on the desorption branch. The catalyst surface area was estimated by the Brunauer-Emmett-Teller (BET) method, through a multi-point BET analysis. SCO particles produced by qUHS and solid-state reaction were imaged by scanning electron microscopy (SEM, JEOL 7800F), high resolution transmission electron microscopy (HR-TEM, JEOL JEM 2100), and transmission electron microscopy energy dispersive X-ray analysis (TEM-EDX) using a JEOL JEM 2100 instrument equipped with EDX (65 mm^2 Oxford Silicon Drift Detector – X-Max). The chemical state of the surface was investigated by XPS using a Kratos Axis Ultra instrument with a monochromatic Al Kα X-ray source. The binding energies were calibrated on the peak of the C-C bond of adventitious carbon (~285 eV). Depth profiling was performed by etching the surface of the material with a 4 kV Ar-ion beam. The etching time was 100 seconds, estimated to result in an etched depth of ~10 nm. By combining XPS with depth profiling, the near-surface and sub-surface of the materials could be analyzed. Soft x-ray absorption spectroscopy (sXAS) was performed at the BL11A beamline of the National Synchrotron Radiation Research Centre (NSRRC) in Taiwan. The Co-$L_{2,3}$ sXAS spectra were recorded in total electron yield mode. To extract the valence and spin states of the Co ions in SCO qUHS, the experimental Co-$L_{2,3}$ edge was simulated by superimposing the spectra of relevant references: CoO for octahedrally coordinated Co^{2+}, $YBaCoFe_3O_7$ for tetrahedrally coordinated Co^{2+} and high-spin (HS) Co^{3+} (upon subtraction from $YBaCo_4O_7$),[16] and $EuCoO_3$ for low-spin (LS) for octahedrally coordinated Co^{3+}.[17] For the SCO conv spectrum simulation, the selected references were $EuCoO_3$ for octahedrally coordinated LS Co^{3+}, Sr_2CoO_3Cl for pyramidally coordinated HS Co^{3+},[17] and $SrCoO_3$ for octahedrally coordinated intermediate-spin (IS) Co^{4+}.[18]

2.3 Electrochemical characterizations

The catalyst ink was prepared by mixing 7 mg of catalyst with 3 mg of Vulcan XC-72 carbon, 0.9 mL of isopropanol, and 0.1 mL of Nafion® (5% perfluorinated solution, Sigma Aldrich). A glassy carbon (GC) electrode was used as the working electrode, while an Ag/AgCl electrode and a graphite rod were used as reference and counter electrodes, respectively. 5 µL of catalyst ink was loaded onto the GC disk surface, resulting in a mass loading of 0.28 mg/cm^2. Catalyst electrochemical performance was evaluated by linear sweep voltammetry (LSV) at a scan rate of 5 mV/s on a rotating disk electrode (RDE, BAS ALS RRDE-3A) using a CHI 900D (CH Instruments Inc.) electrochemical workstation. Unless otherwise specified, measurements were carried out in O_2-saturated 0.1 M KOH solution (pH=13). The resulting data were iR-corrected to compensate for the solution resistance. Electrochemical impedance spectroscopy (EIS) was carried out using a VSP (BioLogic) station from 100 mHz to 100 kHz at 0.8 V *vs* Ag/AgCl in 0.1 M KOH.

3 Results

As outlined in the introduction, brownmillerite SCO has been conventionally sintered by solid-state reaction. Considering the slow heating rate of muffle furnaces (typically set to 5 °C/minute to preserve heating elements) and the calcination time (48 hours), the overall processing time can exceed 50 hours.[9] Using the qUHS apparatus displayed in Figure 1 a), SCO was fabricated in less than 30 seconds (from 15 to 30 seconds), ~10,000 times faster than the conventional route.[9] In the following sections, we will compare the electrochemical and physical properties of the SCO samples fabricated by qUHS and solid-state route.

3.1 OER performance of samples synthesized by qUHS and solid-state route

The electrochemical activity of the materials synthesized by qUHS and solid-state reaction was evaluated using LSV in 0.1 M KOH, see Figure 2 a) and b). SCO prepared by qUHS shows higher OER performance compared to the conventional synthesis route. In particular, the qUHS sample showed higher intrinsic activity (mA/cm^2_{oxide}) and mass activity (mA/mg_{oxide}) over its conventionally sintered counterpart. The origin of this performance improvement was investigated by analyzing and comparing the properties of samples produced by qUHS and solid-state reaction. A selection of the investigated sample properties (*i.e.* sintering time, specific surface area, average pore diameter and volume, and OER specific activity) are outlined in Figure 1 b).

3.2 Samples' structure, porosity, and surface area

XRD analysis of SCO samples produced by solid-state reaction and qUHS both showed a brownmillerite structure (Figure 2 c-e)). The materials synthesized by qUHS seemed to contain a low concentration of $SrCO_3$ impurities, whose presence is corroborated by the more intense carbonate peak in the XPS C 1s spectrum in qUHS SCO (Figure S1). The HR-TEM micrographs in Figure 2 f) show that both crystals are characterized by similar lattice and d-spacing between adjacent fringes. Further, TEM-EDX elemental mapping (see regions marked with A and B in Figure 2 f)) suggests that the qUHS samples might have experienced greater surface Sr segregation compared to the conventionally sintered samples. It is well-known that Sr-based perovskites suffer from surface Sr segregation, leading to the formation of Sr-excess phases such as SrO_x.[10, 19] In addition, severe Sr segregation and SrO_x formation in $La_{0.1}Sr_{0.9}TiO_3$ has been observed in samples produced by flash sintering, which was attributed to the influence of the applied electric field.[10] In our case, Sr segregation may be triggered by the electric field applied to the carbon strips of the qUHS setup as well as by the carbon strips

themselves, whose presence likely generates a reducing environment that is favorable to Sr segregation.[20]

The samples' porosity and surface area were evaluated by N_2 physisorption, obtaining the adsorption and desorption isotherms shown in Figure S2. The analyzed materials are characterized by type V physisorption isotherms with a hysteresis loop of type H1.[21] Interestingly, the qUHS sample shows substantial hysteresis, indicating a greater content of mesopores (*i.e.* pores with diameter in the range of 2-50 nm) with bigger average pore diameter (33.2 nm *vs* 17.74 nm), higher total pore volume (0.145 cm^3/g *vs* 0.006 cm^3/g) relative to the conventional sample. Further, qUHS sample is characterized by higher surface area (0.47 m^2/g) compared to the conventional one (0.39 m^2/g).

3.3 Chemical state of samples' surface

As changes in the surface state have an important influence on electrocatalysis, SCO qUHS and SCO conv were analyzed with surface-sensitive techniques, such as XPS and synchrotron-based sXAS. In addition, XPS measurements were performed at different depths, *i.e.*, the outer layer and after Ar-ion etching, thereby targeting both the sample surface and sub-surface.

First, the chemical state of Sr in the samples was assessed to investigate the cation segregation observed by TEM-EDX. For this purpose, the XPS Sr 3d orbital of the qUHS and conventional samples was analysed. As shown in Figure S3, this orbital is characterized by the presence of doublets, $3d_{3/2}$ and $3d_{5/2}$, due to spin orbit coupling. These spectra can be fitted using two pairs of doublets, where higher energy pair, ≈135.2 eV for $3d_{3/2}$ and ≈133.4 eV for $3d_{5/2}$, has been attributed to surface Sr, while the lower energy doublet, ≈134.48 eV for $3d_{3/2}$ and ≈132.7 eV for $3d_{5/2}$, indicates the presence of lattice Sr.[22] Comparing Figure S3 a) and b), the Sr 3d spectrum of SCO qUHS is characterized by a significant shift towards higher binding energy compared to SCO conv. Such an energy shift indicates the predominance of surface Sr, further

implying that samples sintered by qUHS are characterized by enhanced Sr segregation, consistent with the TEM-EDX results.

The Co 2p and O 1s XPS spectra of the qUHS and conventional samples were analyzed. The Co 2p orbital of SCO qUHS is characterized by the presence of Co^{2+} and Co^{3+} peaks,[23] with strong satellite at 786 eV, typical of Co^{2+}.[24] In contrast, the SCO conv spectrum can be fit to Co^{4+} and Co^{3+}, see Figure 3 a) and b), with a satellite feature around 790 eV, characteristic of Co^{3+}.[25] The area ratio of the performed XPS fitting suggests a lower Co valence state in SCO qUHS (~2.4+) compared to SCO conv (~3.22+). Furthermore, the O 1s spectra of the two samples are remarkably different, see Figure 3 c) and d). In particular, the peak attributed to the hydroxyl group dominates the qUHS sample's spectrum, suggesting more facile OH^- absorption compared to the conventional sample. Improved OH^- adsorption would result in improved mass transport, which is beneficial to OER activity.[26]

The surface electronic structure of SCO conv and SCO qUHS was studied by synchrotron-based sXAS, as the Co-$L_{2,3}$ edge spectra are highly sensitive to Co valence,[27] spin state,[17] and local coordination environment.[16] The experimentally measured Co $L_{3,2}$-edge spectra of SCO conv and qUHS are shown in Figure 3 e) and f). A Co $L_{3,2}$-edge similar to the one observed for SCO qUHS was previously reported for $La_{1.5}Sr_{0.5}CoO_4$,[28] in which the 777.8 eV feature is consistent with octahedrally coordinated Co^{2+}. In contrast, the main peak is located at ~781 eV, matching the Co^{3+} reference (*i.e.* $EuCoO_3$) and indicating mixed Co^{2+} and Co^{3+} in SCO qUHS. The Co valence in SCO qUHS and SCO conv was determined by simulating the experimental Co-$L_{2,3}$ edge through the superposition of relevant reference spectra (details can be found in the Methods section). The simulated Co-$L_{2,3}$ edge spectra (black solid lines in Figure 3 e) and f)) closely match the experimental data, indicating that the Co valence is 2.55+ and 3.33+ for SCO qUHS and SCO conv, respectively. The co-existence of Co^{2+} Td and Co^{3+} Oh in SCO qUHS is beneficial to the OER, as the former has been reported to increase affinity

to oxygen ions, thereby enhancing active site availability.[29] In contrast, SCO conv is dominated by Co^{3+} Oh, which is known to form strong -OH bonds, lowering activity.[29] In addition, sXAS fitting reveals that SCO qUHS is composed of 35% CoO_6 and 65% CoO_4. Conversely, fitting of SCO conv was consistent with 80% CoO_6 and 20% CoO_5 content. It has recently been reported that a 50:50 ratio between different transition metal coordinating environments (*e.g.* 50% CoO_6 and 50% CoO_4) is highly synergistic for OER activity.[25a] Thus, the Co coordination environment at the SCO qUHS surface promotes higher OER activity than in SCO conv.

Sub-surface layers of the materials were also analyzed by XPS, as shown in Figure 4 and S4. The samples produced by qUHS and the conventional route display similar Co 2p orbitals at the sub-surface, with a satellite feature at ≈786 eV, typical of Co^{2+}. Regarding the O 1s spectra, the two materials preserved the differences observed at the surface, as the qUHS sample still has a predominant hydroxyl peak. Concurrently, the peak attributed to lattice oxygen at the sub-surface is stronger in both materials compared to the surface, which is reasonable as the investigated layer is closer to the bulk. Lastly, in contrast to what was observed at the surface, the Sr 3d orbital of both the qUHS and conventional sample is characterized by similar distribution of surface and lattice Sr at the sub-surface, indicating that this region is less affected by Sr segregation.

4 Discussion

The materials produced by qUHS show distinct characteristics from those of conventional samples, including porosity, surface area, and surface chemical state. Unraveling the accompanied improvements in OER activity for the qUHS sample is key to furthering the understanding and development of rapid sintering techniques for electrocatalyst production.

4.1 OER performance enhancement: role of surface chemical state and porosity

In light of the characterizations discussed above, the high OER activity of the qUHS sample is probably due to the synergistic effect between its surface state and mesoporosity. XPS and sXAS characterizations suggest that the surface chemical state of SCO qUHS is likely beneficial to the OER. In fact, the percentage of Co sites with CoO_6 and CoO_4 coordination (65% and 35%, respectively) is thought to benefit OER performance.[25a] In addition, SCO qUHS seems to be characterized by improved OH^- uptake compared to the conventional sample. We further compared the materials' ability to adsorb OH^- from alkaline solutions by FT-IR measurements after exposure to 0.1 M KOH, as reported in reports in the literature,[26, 30] see Figure S5. The IR band centered at a wavenumber of ~3400 cm^{-1} corresponds to the stretching vibrations of OH^- groups. The material fabricated by qUHS, compared to the conventional sample, exhibits stronger OH^- band, corroborating the improved OH^- uptake.

Concurrently, the mesoporosity of the qUHS sample may be essential for enhancing OER performance, as mesopores can enhance access to active sites,[31] resulting in faster reaction.[32] The enhanced accessibility to the active sites is also supported by the augmented electrochemical surface area (ECSA) of the qUHS sample compared to that of SCO conv, see Figure S6, which could help to explain the higher specific OER activity and mass activity of the qUHS materials.

4.2 OER performance enhancement: influence of post and pre-synthesis treatments and conditions

To further improve the performance of qUHS SCO, further enhancements in the enriched surface and specific surface area were targeted. To achieve this, qUHS and solid-state reaction synthesized materials were modified following three different strategies.

4.2.1 Acid etching

Firstly, Sr segregation was mitigated by treating the SCO qUHS and SCO conv powders in 0.1 M HNO_3. The surface Sr-rich layer is characterized by strong oxygen binding, low reactivity, and low electrical conductivity [33] and acid treatment can effectively remove these Sr-O bonds. EIS measurements in Figure S7 a) show that the as-synthesized SCO qUHS has significantly higher charge transfer resistance compared to SCO conv, imputable to Sr segregation and higher Co^{2+} ion content.[34] In contrast, the etched materials display comparable charge transfer resistance, see Figure S7 b). Consistently, the Sr 3d XPS spectra of the etched materials in Figure S8 a) and b) show similar Sr distribution at surface and lattice, implying that SCO qUHS is no longer characterized by prevalence of surface Sr. In addition, the Co 2p orbitals in Figure S8 c) and d) suggest that also after etching SCO qUHS is likely characterized by lower Co valence state compared to SCO conv. Finally, the O 1s spectra in Figure S8 e) and f), show that upon etching, SCO qUHS maintains a more intense hydroxyl peak compared to SCO conv. Concurrently, the intensity of the peak attributed to superoxidative oxygen increased after etching for both materials, consistent with previous reports.[35] Electrochemical characterizations show that after etching, SCO qUHS is characterized by high performance, and maintains higher catalytic activity compared to the conventional sample see Figure 5 a). Then, the etched SCO samples were tested at different KOH concentrations, in experimental conditions ranging from pH=12.5 to pH=14, which can help to elucidate the role of mass transport. In Figure 5 c), the current density collected at 1.7 V *vs* RHE at each tested pH is presented. These results demonstrate that the higher pH, the higher the mobility of OH^- ions, and the bigger the difference in OER performance between the qUHS and conventional samples. As a result, in a 1 M KOH electrolyte (pH=14) the enhanced mass transport of the qUHS sample becomes essential, resulting in substantially higher OER performance compared to the conventional sample, see Figure 5 b). These results seem to corroborate the activity

improvement mechanism hypothesized previously; the improved OH^- adsorption and enhanced mesoporosity of the qUHS sample result in enhanced accessibility to the OER active sites and mass transport, thereby leading to higher activity. The stability of the catalytic activity of the material fabricated by qUHS was also assessed. As shown in Figure S9, the sample did not experience any decay in OER activity, delivering a steady current density at 1.65 V *vs* RHE for more than 10,000 s.

4.2.2 Post-synthesis high-energy ball-milling

As a second strategy, the materials' specific surface area was enhanced by post-synthesis high-energy ball-milling, hereafter denoted as "milled" materials. The materials were milled for 24 hours and the obtained specific surface area was ~30 m^2/g. Figure 6 a) highlights the stark contrast between the as-synthesized SCO conv and milled SCO qUHS, displaying the enormous improvement that can be obtained by simply combining qUHS and post-synthesis milling. Furthermore, Figure 6 b) and Figure S10 indicate that SCO qUHS has higher mass and surface specific activity than SCO conv, in both as-synthesized and post-synthesis milled forms.

4.2.3 Influence of different pre-sintering conditions

Finally, the effect of different pre-sintering conditions was explored, *i.e.*, the precursor grinding (using two different ball-millers, resulting in finer, if high-energy ball-milled, or coarser precursors powders) and pellet pressing method (either uniaxial or isostatic pressing). The adopted experimental design is commented in the SI and schematically represented in Figure S11. From the LSV curves in Figure S12, the materials prepared by qUHS consistently show higher performance throughout the experimental design compared to those sintered conventionally. In addition, the materials prepared with fine precursors (denoted with HB) have higher activity compared to those prepared with coarser precursors, especially if SCO qUHS is used. Conversely, pellet preparation by isostatic or uniaxial press does not have a significant

impact on the OER performance. Porosity, surface area, and particles' size of the samples were analyzed. As detailed in the SI, see Figure S13 and S14, DLS measurements and SEM imaging suggest that particles of qUHS samples are significantly smaller. The samples' surface area is 15 times higher if precursors are high-energy ball-milled and qUHS is used (15.18 m^2/g *vs* 1.09 m^2/g using qUHS and solid-state reaction, respectively), see Figure S15. Therefore, precursor grinding has significant influence on particles' size and surface area if qUHS is used, as its short timescale prevents coarsening. Similarly, the sample porosity increases when high-energy ball-milled precursors are used (2.535 cm^3/g *vs* 0.023 cm^3/g total pore volume for qUHS and solid-state reaction sample, respectively), see Table S2. In contrast, isostatic pressing enables a shorter sintering time (~15 s), likely due to higher contact area between particles which might enhance the sintering rate.

5 Conclusions

In this work, brownmillerite SCO was successfully synthesized by qUHS, a process consisting of rapid sintering and quenching, leading to a substantial reduction of processing time. Furthermore, the sample produced by qUHS was characterized by higher OER performance compared to SCO produced by solid-state reaction. To unravel the origin of this higher activity the properties of the two samples were compared.

The surface of the sample produced by qUHS is affected by enhanced Sr segregation compared to conventionally sintered SCO, as observed by TEM-EDX and XPS. The qUHS sample is also characterized by a different Co chemical state at the surface. In particular, SCO qUHS shows similar proportions of CoO_4 and CoO_6, which are likely to enhance OER activity synergistically.[25a] Further, SCO qUHS possesses an enhanced network of mesopores compared to the conventional SCO. In addition, XPS, sXAS, and FT-IR suggest that SCO qUHS can adsorb OH^- more easily. The combination of mesoporosity and favorable OH^-

uptake is particularly beneficial to OER; hydroxyls are readily adsorbed from the electrolyte and mesopores can enhance ionic transport. Hence, access to the catalyst's active sites is facilitated, resulting in increased ECSA.

The performance of the material was further augmented by post-synthesis treatments, *i.e.*, acid etching and post-synthesis milling, and the modification of pre-sintering conditions, *i.e.*, precursor grinding and pellet pressing method. In particular, OER activity of etched SCO qUHS and conv samples differed more significantly with increasing pH, implying that improved mass transport becomes essential when more OH^- ions are available in the electrolyte.

In conclusion, the properties of electrocatalysts produced by ultrafast sintering and solid-state reaction were compared for the first time, and a possible mechanism involved in activity improvement was proposed. These insights demonstrate the suitability of qUHS/UHS for the exploration of novel materials and rapid production of established electrocatalysts with enhanced properties.

Acknowledgments

The authors gratefully acknowledge the Research Grant Council of Hong Kong for support through the projects (16201820 and 16206019). A. Curcio, M. J. Robson, and A. Belotti kindly recognize the support of the Hong Kong Ph.D. Fellowship Scheme. The authors would like to acknowledge the Materials Preparation and Characterization Facility (MCPF) and the Advanced Engineering Materials Facility (AEMF). Finally, we acknowledge support from the Max Planck-POSTECH-Hsinchu Center for Complex Phase Materials.

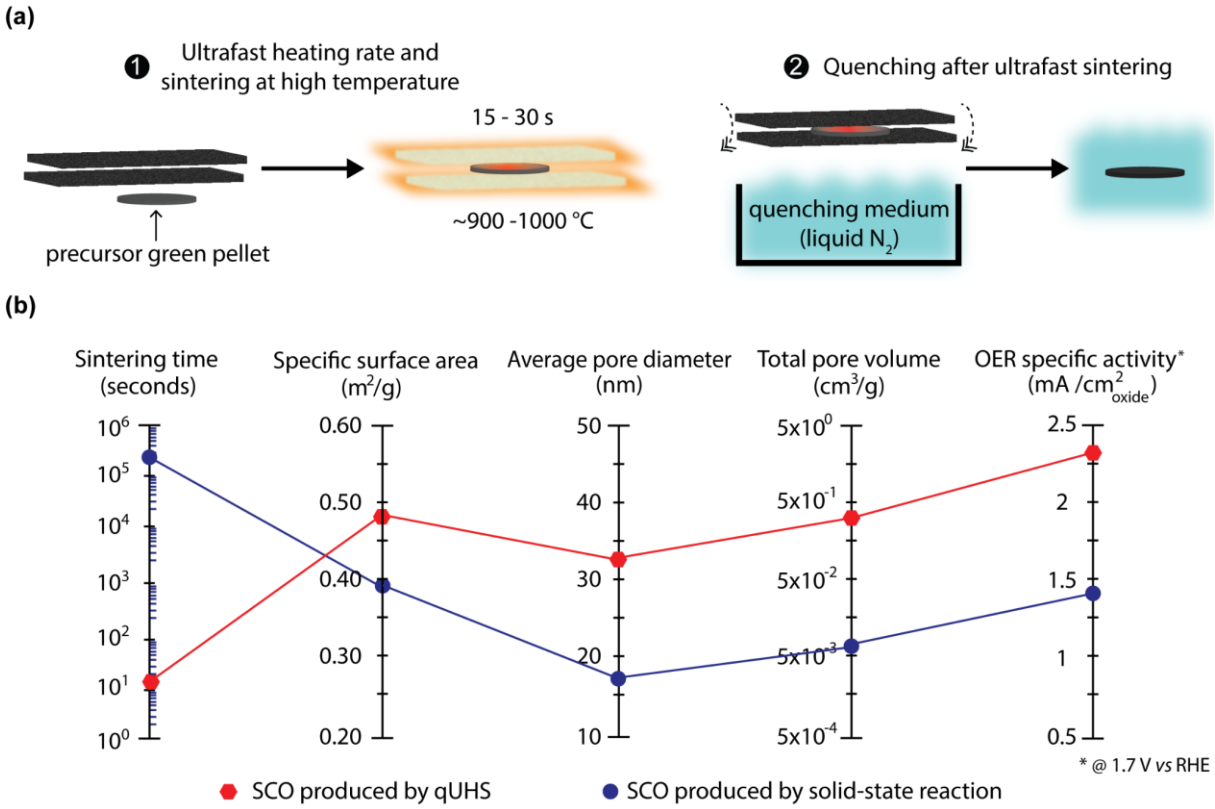

Figure 1. a) schematics of the qUHS procedure. b) comparison of some key features of the SCO samples synthesized using qUHS and the conventional solid-state reaction, SCO qUHS and SCO conv, respectively.

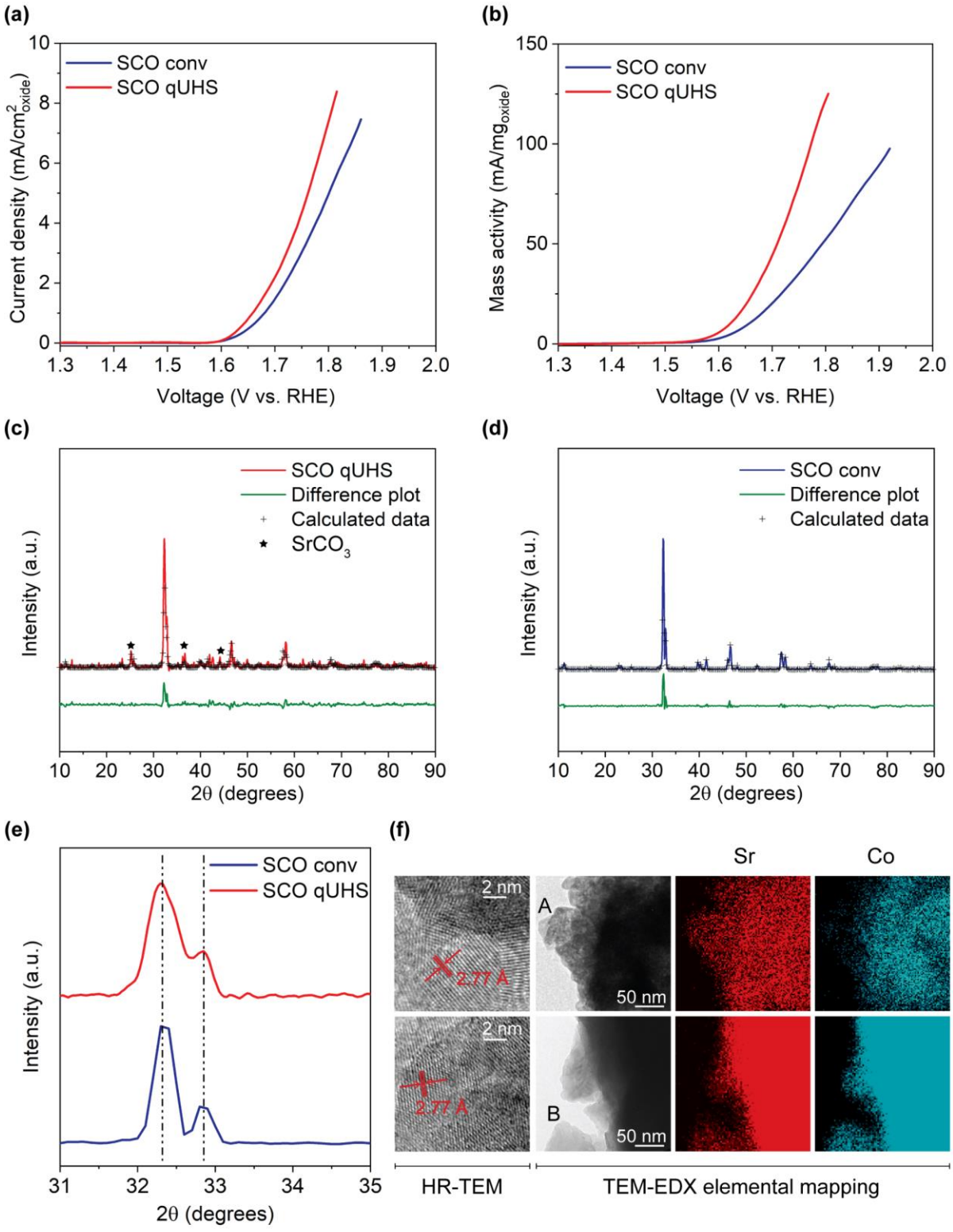

Figure 2. a) and b), specific and mass activity of the as-synthesized SCO conv and SCO qUHS c) and d), XRD pattern, calculated patterns by Rietveld refinement, and the respective difference plots of SCO qUHS and SCO conv samples. e) Magnified region surrounding the

main peak of the XRD pattern of the two materials, showing the characteristic peak of the brownmillerite phase. f) HR-TEM micrographs and TEM-EDX elemental mapping of the qUHS (top row) and conventional sample (bottom row).

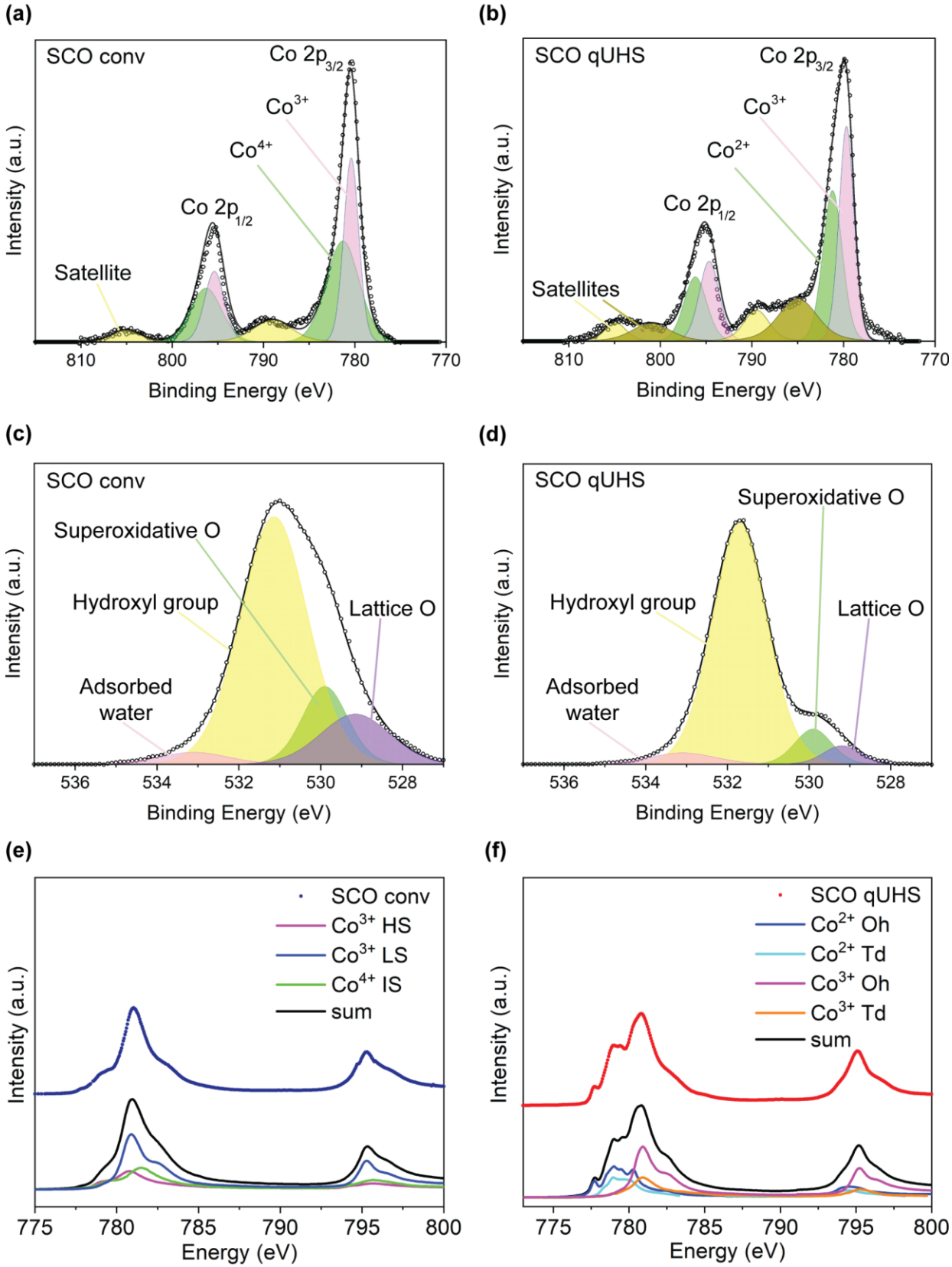

Figure 3. XPS spectra of Co 2p (a) and b)), and O 1s (c) and d)) of SCO conv and qUHS collected at the surface. e-f) measured and simulated Co $L_{3,2}$-edge sXAS spectra of the two

samples. The valence state of Co for SCO qUHS is 2.55+ and 3.33+ for SCO conv. HS, LS, and IS denote high-spin, low-spin, and intermediate-spin, respectively. Oh and Td indicate octahedral and tetrahedral, respectively.

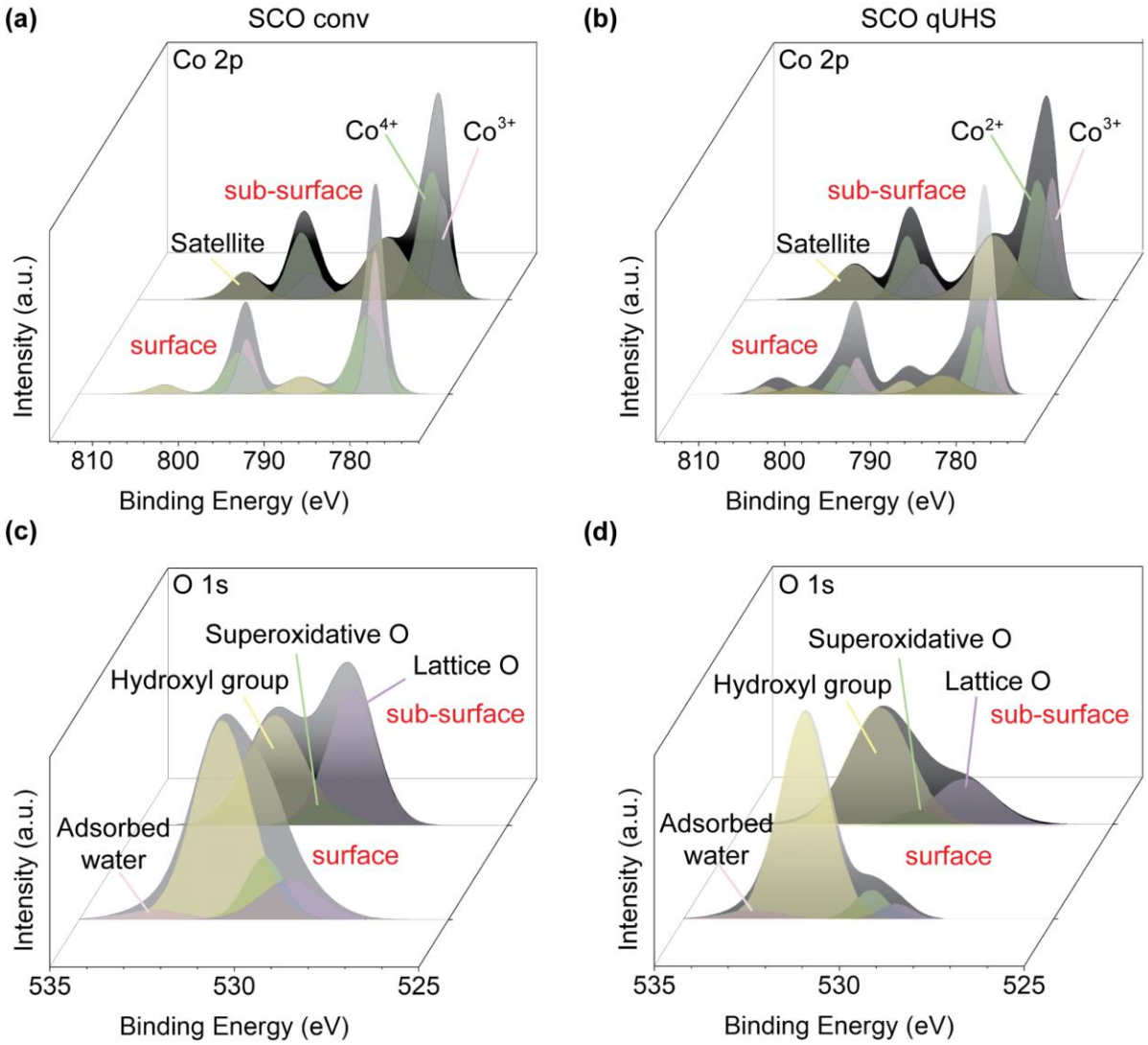

Figure 4. XPS depth profiling of SCO samples synthesized by the conventional solid-state route (left-hand side panels, a) and c)) and qUHS (right-hand side panels, b) and d)). XPS was performed at the surface layer and at the sub-surface layer (depth ~10 nm after ion beam etching) of the sample.

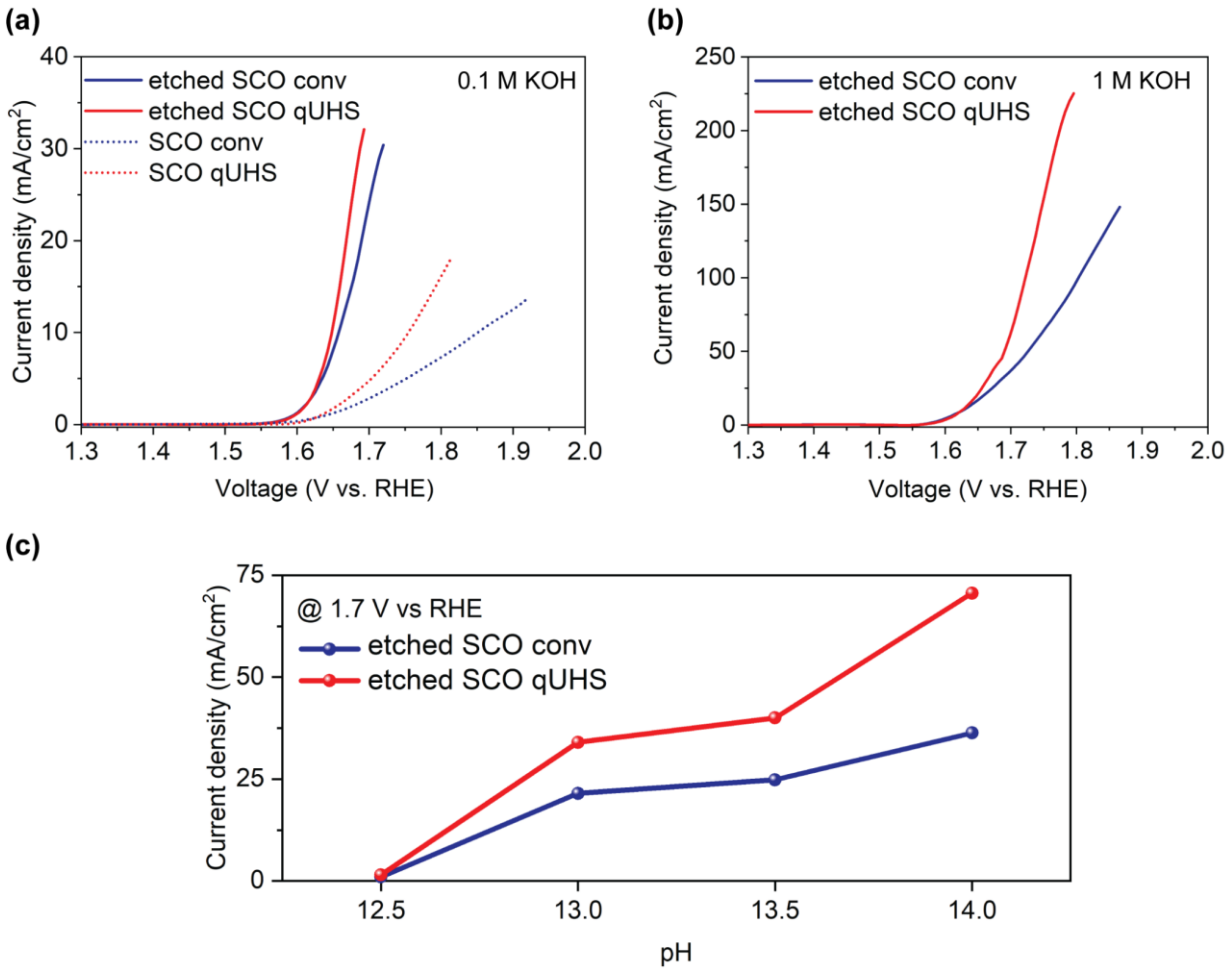

Figure 5. a) OER LSV in 0.1M KOH of SCO conv and SCO qUHS before (dotted line) and after (solid line) etching in 0.1M HNO_3. b) OER LSV in 1M KOH of SCO conv and SCO qUHS after etching. c) plot of the current density registered at 1.7 V vs. RHE for SCO conv and SCO qUHS, which shows how the difference in electrochemical activity becomes remarkable varying the pH from 12.5 to 14.

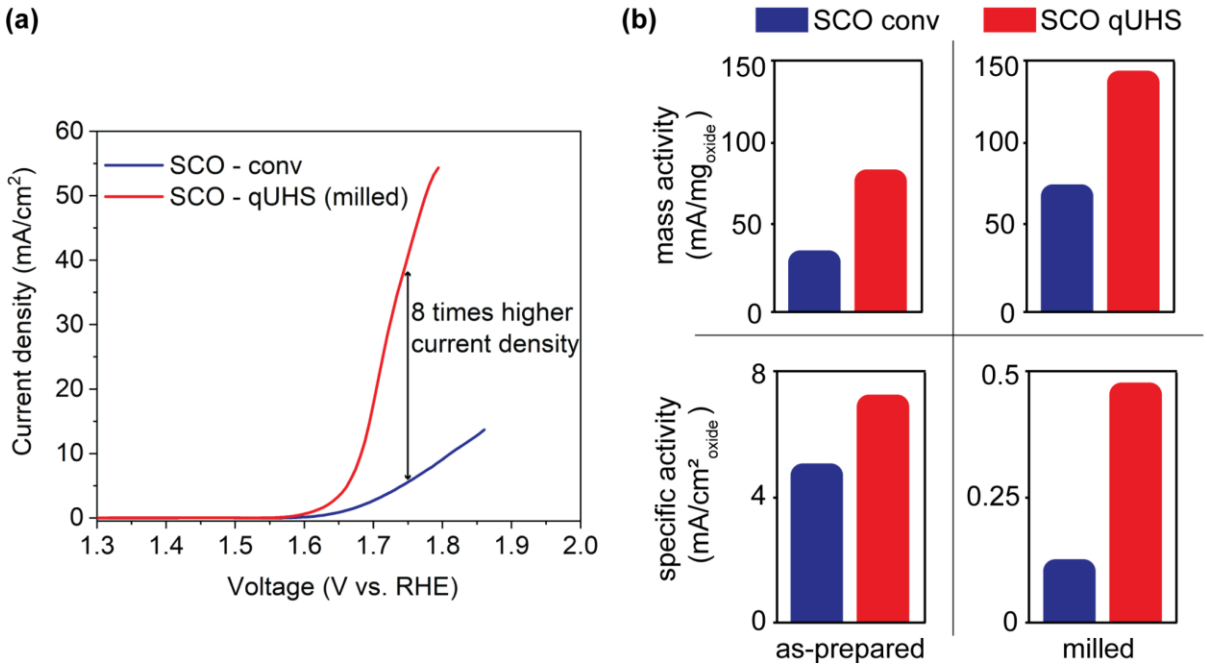

Figure 6. a) comparison of measured current density of SCO qUHS (upon post-synthesis milling) and SCO conv, highlighting the evident improvement in the material's performance. b) table comparing OER specific and mass activity of SCO conv and SCO qUHS

References

[1] R.-F. Guo, H.-R. Mao, Z.-T. Zhao, P. Shen, *Scripta Materialia* **2021**, 193, 103.

[2] T. Ibn-Mohammed, C. A. Randall, K. B. Mustapha, J. Guo, J. Walker, S. Berbano, S. C. L. Koh, D. Wang, D. C. Sinclair, I. M. Reaney, *Journal of the European Ceramic Society* **2019**, 39, 5213.

[3] a) M. Biesuz, V. M. Sglavo, *Journal of the European Ceramic Society* **2019**, 39, 115; b) M. Kermani, M. Biesuz, J. Dong, H. Deng, M. Bortolotti, A. Chiappini, M. J. Reece, V. M. Sglavo, C. Hu, S. Grasso, *Journal of the European Ceramic Society* **2020**, 40, 6266.

[4] M. Oghbaei, O. Mirzaee, *Journal of Alloys and Compounds* **2010**, 494, 175.

[5] O. Guillon, J. Gonzalez-Julian, B. Dargatz, T. Kessel, G. Schierning, J. Räthel, M. Herrmann, *Advanced Engineering Materials* **2014**, 16, 830.

[6] a) J. Guo, H. Guo, A. L. Baker, M. T. Lanagan, E. R. Kupp, G. L. Messing, C. A. Randall, *Angewandte Chemie International Edition* **2016**, 55, 11457; b) S. Grasso, M. Biesuz, L. Zoli, G. Taveri, A. I. Duff, D. Ke, A. Jiang, M. J. Reece, *Advances in Applied Ceramics* **2020**, 119, 115; c) J. Guo, S. S. Berbano, H. Guo, A. L. Baker, M. T. Lanagan, C. A. Randall, *Advanced Functional Materials* **2016**, 26, 7115.

[7] C. Wang, W. Ping, Q. Bai, H. Cui, R. Hensleigh, R. Wang, A. H. Brozena, Z. Xu, J. Dai, Y. Pei, C. Zheng, G. Pastel, J. Gao, X. Wang, H. Wang, J.-C. Zhao, B. Yang, X. Zheng, J. Luo, Y. Mo, B. Dunn, L. Hu, *Science* **2020**, 368, 521.

[8] Y. Lin, N. Luo, E. Quattrocchi, F. Ciucci, J. Wu, M. Kermani, J. Dong, C. Hu, S. Grasso, *Ceramics International* **2021**, 47, 21982.

[9] Y. Takeda, R. Kanno, T. Takada, O. Yamamoto, M. Takano, Y. Bando, *Zeitschrift für anorganische und allgemeine Chemie* **1986**, 540, 259.

[10] B. Kayaalp, K. Klauke, M. Biesuz, A. Iannaci, V. M. Sglavo, M. D'Arienzo, H. Noei, S. Lee, W. Jung, S. Mascotto, *The Journal of Physical Chemistry C* **2019**, 123, 16883.

[11] M. A. Naseer, M. K. Tufail, A. Ali, S. Hussain, U. Khan, H. Jin, *Journal of The Electrochemical Society* **2021**, 168, 060529.

[12] C. Liu, J. Qian, Y. Ye, H. Zhou, C.-J. Sun, C. Sheehan, Z. Zhang, G. Wan, Y.-S. Liu, J. Guo, S. Li, H. Shin, S. Hwang, T. B. Gunnoe, W. A. Goddard, S. Zhang, *Nature Catalysis* **2021**, 4, 36.

[13] E. Fabbri, A. Habereder, K. Waltar, R. Kötz, T. J. Schmidt, *Catalysis Science & Technology* **2014**, 4, 3800.

[14] a) J.-C. Grenier, S. Ghodbane, G. Demazeau, M. Pouchard, P. Hagenmuller, *Materials Research Bulletin* **1979**, 14, 831; b) B. Han, A. Grimaud, L. Giordano, W. T. Hong, O. Diaz-Morales, L. Yueh-Lin, J. Hwang, N. Charles, K. A. Stoerzinger, W. Yang, M. T. M. Koper, Y. Shao-Horn, *The Journal of Physical Chemistry C* **2018**, 122, 8445; c) Y. Long, Y. Kaneko, S. Ishiwata, Y. Taguchi, Y. Tokura, *Journal of Physics: Condensed Matter* **2011**, 23, 245601; d) P. Bezdicka, A. Wattiaux, J. C. Grenier, M. Pouchard, P. Hagenmuller, *Zeitschrift für anorganische und allgemeine Chemie* **1993**, 619, 7; e) Y. Ito, R. F. Klie, N. D. Browning, T. J. Mazanec, *Journal of the American Ceramic Society* **2002**, 85, 969; f) O. Jankovský, D. Sedmidubský, J. Vítek, P. Šimek, Z. Sofer, *Journal of the European Ceramic Society* **2015**, 35, 935; g) J. Rodríguez, J. M. González-Calbet, *Materials Research Bulletin* **1986**, 21, 429; h) A. Grimaud, O. Diaz-Morales, B. Han, W. T. Hong, Y.-L. Lee, L. Giordano, K. A. Stoerzinger, M. T. M. Koper, Y. Shao-Horn, *Nature Chemistry* **2017**, 9, 457; i) A. Curcio, J. Wang, Z. Wang, Z. Zhang, A. Belotti, S. Pepe, M. B. Effat, Z. Shao, J. Lim, F. Ciucci, *Advanced Functional Materials* **2021**, 31, 2008077.

[15] a) A. Muñoz, C. de la Calle, J. A. Alonso, P. M. Botta, V. Pardo, D. Baldomir, J. Rivas, *Physical Review B* **2008**, 78, 054404; b) C. de la Calle, A. Aguadero, J. A. Alonso, M. T. Fernández-Díaz, *Solid State Sciences* **2008**, 10, 1924; c) X. Chen, M. Kubota, S. Yamashita, H. Kita, *Journal of Energy Storage* **2021**, 38, 102501.
[16] N. Hollmann, Z. Hu, M. Valldor, A. Maignan, A. Tanaka, H. H. Hsieh, H. J. Lin, C. T. Chen, L. H. Tjeng, *Physical Review B* **2009**, 80, 085111.
[17] Z. Hu, H. Wu, M. W. Haverkort, H. H. Hsieh, H. J. Lin, T. Lorenz, J. Baier, A. Reichl, I. Bonn, C. Felser, A. Tanaka, C. T. Chen, L. H. Tjeng, *Physical Review Letters* **2004**, 92, 207402.
[18] R. H. Potze, G. A. Sawatzky, M. Abbate, *Physical Review B* **1995**, 51, 11501.
[19] B. Koo, K. Kim, J. K. Kim, H. Kwon, J. W. Han, W. Jung, *Joule* **2018**, 2, 1476.
[20] T. T. Fister, D. D. Fong, J. A. Eastman, P. M. Baldo, M. J. Highland, P. H. Fuoss, K. R. Balasubramaniam, J. C. Meador, P. A. Salvador, *Applied Physics Letters* **2008**, 93, 151904.
[21] M. Thommes, K. Kaneko, A. V. Neimark, J. P. Olivier, F. Rodriguez-Reinoso, J. Rouquerol, K. S. W. Sing, *Pure and Applied Chemistry* **2015**, 87, 1051.
[22] E. J. Crumlin, E. Mutoro, Z. Liu, M. E. Grass, M. D. Biegalski, Y.-L. Lee, D. Morgan, H. M. Christen, H. Bluhm, Y. Shao-Horn, *Energy & Environmental Science* **2012**, 5, 6081.
[23] M. N. Ha, G. Lu, Z. Liu, L. Wang, Z. Zhao, *Journal of Materials Chemistry A* **2016**, 4, 13155.
[24] Z. Cai, M. Kubicek, J. Fleig, B. Yildiz, *Chemistry of Materials* **2012**, 24, 1116.
[25] a) L. Li, H. Sun, Z. Hu, J. Zhou, Y.-C. Huang, H. Huang, S. Song, C.-W. Pao, Y.-C. Chang, A. C. Komarek, H.-J. Lin, C.-T. Chen, C.-L. Dong, J.-Q. Wang, L. Zhang, *Advanced Functional Materials* **2021**, n/a, 2104746; b) L. Dahéron, R. Dedryvère, H. Martinez, M. Ménétrier, C. Denage, C. Delmas, D. Gonbeau, *Chemistry of Materials* **2008**, 20, 583.
[26] S. She, Y. Zhu, H. A. Tahini, Z. Hu, S.-C. Weng, X. Wu, Y. Chen, D. Guan, Y. Song, J. Dai, S. C. Smith, H. Wang, W. Zhou, Z. Shao, *Applied Physics Reviews* **2021**, 8, 011407.
[27] Y. Y. Chin, Z. Hu, H. J. Lin, S. Agrestini, J. Weinen, C. Martin, S. Hébert, A. Maignan, A. Tanaka, J. C. Cezar, N. B. Brookes, Y. F. Liao, K. D. Tsuei, C. T. Chen, D. I. Khomskii, L. H. Tjeng, *Physical Review B* **2019**, 100, 205139.
[28] C. F. Chang, Z. Hu, H. Wu, T. Burnus, N. Hollmann, M. Benomar, T. Lorenz, A. Tanaka, H. J. Lin, H. H. Hsieh, C. T. Chen, L. H. Tjeng, *Physical Review Letters* **2009**, 102, 116401.
[29] H.-Y. Wang, S.-F. Hung, H.-Y. Chen, T.-S. Chan, H. M. Chen, B. Liu, *Journal of the American Chemical Society* **2016**, 138, 36.
[30] X. Xu, C. Su, W. Zhou, Y. Zhu, Y. Chen, Z. Shao, *Advanced Science* **2016**, 3, 1500187.
[31] J. Qi, W. Zhang, R. Cao, *ChemCatChem* **2018**, 10, 1206.
[32] G. Chen, Y. Zhu, H. M. Chen, Z. Hu, S.-F. Hung, N. Ma, J. Dai, H.-J. Lin, C.-T. Chen, W. Zhou, Z. Shao, *Advanced Materials* **2019**, 31, 1900883.
[33] W. Jung, H. L. Tuller, *Energy & Environmental Science* **2012**, 5, 5370.
[34] Q. Lin, Y. Zhu, Z. Hu, Y. Yin, H.-J. Lin, C.-T. Chen, X. Zhang, Z. Shao, H. Wang, *Journal of Materials Chemistry A* **2020**, 8, 6480.
[35] a) X. Wang, K. Huang, L. Yuan, S. Xi, W. Yan, Z. Geng, Y. Cong, Y. Sun, H. Tan, X. Wu, L. Li, S. Feng, *The Journal of Physical Chemistry Letters* **2018**, 9, 4146; b) W. Guo, L. Cui, H. Xu, C. Gong, *Applied Surface Science* **2020**, 529, 147165.